

USE OF TWO-STEP SPLIT-OPERATOR APPROACH FOR 2D SHALLOW WATER FLOW COMPUTATION

HO-CHENG LIEN*, TE-YUNG HSIEH AND JINN-CHUANG YANG

Department of Civil Engineering, National Chiao Tung University, 1001 Ta Hsueh Road, Hsinchu, 30050, Taiwan, Republic of China

SUMMARY

The objective of this paper is to present a methodology of using a two-step split-operator approach for solving the shallow water flow equations in terms of an orthogonal curvilinear co-ordinate system. This approach is in fact one kind of the so-called fractional step method that has been popularly used for computations of dynamic flow. By following that the momentum equations are decomposed into two portions, the computation procedure involves two steps. The first step (dispersion step) is to compute the provisional velocity in the momentum equation without the pressure gradient. The second step (propagation step) is to correct the provisional velocity by considering a divergence-free velocity field, including the effect of the pressure gradient. This newly proposed method, other than the conventional split-operator methods, such as the projection method, considers the effects of pressure gradient and bed friction in the second step. The advantage of this treatment is that it increases flexibility, efficiency and applicability of numerical simulation for various hydraulic problems. Four cases, including back-water flow, reverse flow, circular basin flow and unsteady flow, have been demonstrated to show the accuracy and practical application of the method. Copyright © 1999 John Wiley & Sons, Ltd.

KEY WORDS: two-step split-operator approach; fractional step method; projection method; shallow water flow equations; numerical simulation

1. INTRODUCTION

For hydraulic engineers, the use of depth-averaged 2D models for solving shallow water flow equations to deal with the relevant hydraulic problems is gradually getting popular owing to their efficiency and reasonable accuracy. These models are valid when the width-to-depth ratio is large and the vertical variation of the mean flow equations is not significant because of strong vertical mixing by the fully turbulent effects. The finite difference method (FDM) is the most popular numerical scheme for developing the depth-averaged 2D models. Several kinds of solution algorithms using FDM had been proposed, such as the three-level implicit scheme by Falconer [1], the staggered leap-frog method by Takahashi and Nakagawa [2], the Beam and Warming method by Molls and Chaudhry [3], the three-step split-operator approach by Benque *et al.* [4], and the two-step implicit algorithm by Ye and McCorquodale [5].

* Correspondence to: Department of Civil Engineering, National Chiao Tung University, 1001 Ta Hsueh Road, Hsinchu, 30050, Taiwan, Republic of China. Fax: + 886 3 5727241; e-mail: u8116541@cc.nctu.edu.tw

Contract/grant sponsor: National Science Council of Taiwan, Republic of China; Contract/grant number: NSC-84-2211-E009-033

The split-operator approach, which is one kind of the projection method [6], is a popular solution algorithm for solving the time-accurate incompressible Navier–Stokes equations with primitive variables [7,8]. For pressure flows it is difficult to determine the pressure field because of the lack of a relationship between velocity and pressure. One of the practical uses, such as SIMPLE [9] method, is to guess the pressure field first, then correct it as a newly guessed pressure repeatedly until a converged solution is obtained. In Rosenfeld and Kwak's [10] research, such methods consume a lot of CPU time for many iterations between velocity and the pressure field at each time level. However, the projection method split the momentum equation into two parts: one without pressure gradient and the other with pressure gradient. Thus, the Poisson equation can be derived in correspondence with pressure as a dependent variable. For large numbers of mesh point computation, the iterations in this kind of two-step split-operator approach are usually performed on a single equation (pressure equation) rather than on a set of equations as in the SIMPLE method, so it can accelerate the convergence rate and reduce the consumption of CPU time.

The major concept in a split-operator approach is to decompose the momentum equation to solve the linked pressure–velocity problem. Though shallow water flow equations have no such problem because of introducing the assumption of static pressure distribution over depth, the split-operator approach still had to be used to develop the depth-averaged 2D model. Benque *et al.* [4] was the first to use this concept for the computation of 2D tidal current flow in the bay or estuary. They proposed three-step split-operator approach, i.e. advection step, diffusion step and propagation step, in which momentum advection is calculated using the method of characteristics, horizontal momentum diffusion is calculated using an implicit finite difference scheme, and wave propagation is calculated using an iterative alternating direction implicit (ADI) method. The objectives of their research were to overcome the numerical attenuation, parasitic oscillation, and poor reproduction of wave propagation because of using the ADI method with the large time step. So they used proper numerical schemes to solve the different types of partial differential equation appearing in the momentum equation. Lately, Spasojevic and Holly [11] extended the numerical algorithm of the Benque *et al.*'s model to solve the flow and sediment equations. Ye and McCorquodale [5] developed a fractional two-step implicit algorithm to solve several open channel flows, including pure convection of a sharp step profile, side discharge into a channel, and flow in a Parshall flume with supercritical outflow. They used the power law scheme based on the SIMPLEC [12] to solve the provisional velocity implicitly in the first step (convection–diffusion process).

One of drawbacks existing in the aforementioned implicit scheme for solving the provisional velocity in the first step is that it is hard to specify the provisional velocity at the boundary in the incomplete momentum equations. The different provisional velocity at the boundary will affect the accuracy of solution for the final velocity and flow depth in the propagation step. Obviously, the three-step split-operator approach is more difficult to determine the provisional velocity at the boundary than the two-step one. Therefore, reducing the three-step procedure to the two-step and using an explicit scheme for solving provisional velocity in the first step are the feasible ways to avoid this deficiency [13]. For order of magnitude analysis, the bed friction is a dominating shear stress in the shallow water flow equations. Benque *et al.* considered not only the pressure gradient but also the bed friction in the propagation step rather than just the conventional projection method. This study adopted this concept but with different split forms, to increase the flexibility of numerical simulation for various hydraulic problems.

The purpose of this paper is to present a new two-step split-operator approach for solving the shallow water flow equations, in which the provisional velocity is computed explicitly in the dispersion step, then the incomplete momentum equation, which contains the pressure

gradient and bed friction, is coupled with the continuity equation in the propagation step to calculate the corrected velocity and the flow depth. Four cases, including back-water flow, reverse flow, circular basin flow and unsteady flow, have been demonstrated to show the flexibility and practical application of the method. For the cases of back-water flow and unsteady flow, when the effect of convection is weak, only one step, the propagation step, is needed to be performed. The cases of reverse flow and circular basin flow demonstrate the need of performing a two-step computation. With the cases demonstrated, the flexibility and the applicability of the newly proposed two-step split-operator approach for 2D shallow water flow computations are presented in this paper.

2. MATHEMATICAL FORMULATION

2.1. Governing equations in orthogonal curvilinear co-ordinates

Under the assumption of incompressible fluid with constant viscosity, the basic equations of fluid dynamics for continuity and motion in vector form can be written as follows:

$$\nabla \cdot \vec{v} = 0, \tag{1}$$

$$\frac{\partial \vec{v}}{\partial t} + (\vec{v} \cdot \nabla) \vec{v} = \frac{1}{\rho} \vec{F} - \frac{1}{\rho} \nabla P + \frac{1}{\rho} \nabla \cdot \underline{\underline{\tau}}, \tag{2}$$

where \vec{v} is the velocity vector; ρ , the fluid density; t , the time; F , the body force; P , the pressure; $\underline{\underline{\tau}}$, the shear-stress tensor.

The basic elements of the co-ordinate transformations and the derivation of the basic equations in orthogonal curvilinear co-ordinates have been briefly introduced by Anderson *et al.* [14]. Let ξ and η be the orthogonal curvilinear co-ordinates in the horizontal plane, and the third co-ordinate direction z has to be a straight vertical line. Since the untransformed z -direction is straight, then the metric coefficient in the z -direction, i.e. h_3 , equals unity and its derivatives with respect to ξ - and η -directions will disappear. Furthermore, the metric coefficients h_1 and h_2 in the ξ - and η -directions depend only on ξ and η , therefore, their derivatives with respect to z should also vanish. It seems tedious to transform Equations (1) and (2) in the boundary fitted orthogonal curvilinear co-ordinate system. So that no details concerning the derivation will be described here. The transformed equations are briefly stated as follows:

Continuity equation:

$$\frac{\partial}{\partial \xi} (h_2 u) + \frac{\partial}{\partial \eta} (h_1 v) + \frac{\partial}{\partial z} (h_1 h_2 w) = 0. \tag{3}$$

Momentum equations:

ξ -direction

$$\begin{aligned} & \frac{\partial u}{\partial t} + \frac{u}{h_1} \frac{\partial u}{\partial \xi} + \frac{v}{h_2} \frac{\partial u}{\partial \eta} + w \frac{\partial u}{\partial z} + \frac{1}{h_1 h_2} \frac{\partial h_1}{\partial \eta} u v - \frac{1}{h_1 h_2} \frac{\partial h_2}{\partial \xi} v^2 \\ & = -\frac{g}{h_1} \frac{\partial}{\partial \xi} \left(z + \frac{P}{\rho g} \right) + \frac{1}{\rho h_1 h_2} \left[\frac{\partial}{\partial \xi} (h_2 \tau_{\xi\xi}) + \frac{\partial}{\partial \eta} (h_1 \tau_{\xi\eta}) + \frac{\partial}{\partial z} (h_1 h_2 \tau_{\xi z}) \right] + \frac{1}{\rho h_1 h_2} \frac{\partial h_1}{\partial \eta} \tau_{\xi\eta} \\ & \quad - \frac{1}{\rho h_1 h_2} \frac{\partial h_2}{\partial \xi} \tau_{\eta\eta}, \end{aligned} \tag{4}$$

η -direction

$$\begin{aligned} & \frac{\partial v}{\partial t} + \frac{u}{h_1} \frac{\partial v}{\partial \xi} + \frac{v}{h_2} \frac{\partial v}{\partial \eta} + w \frac{\partial v}{\partial z} + \frac{1}{h_1 h_2} \frac{\partial h_2}{\partial \xi} u v - \frac{1}{h_1 h_2} \frac{\partial h_1}{\partial \eta} u^2 \\ &= -\frac{g}{h_2} \frac{\partial}{\partial \eta} \left(z + \frac{P}{\rho g} \right) + \frac{1}{\rho h_1 h_2} \left[\frac{\partial}{\partial \xi} (h_2 \tau_{\eta \xi}) + \frac{\partial}{\partial \eta} (h_1 \tau_{\eta \eta}) + \frac{\partial}{\partial z} (h_1 h_2 \tau_{\eta z}) \right] - \frac{1}{\rho h_1 h_2} \frac{\partial h_1}{\partial \eta} \tau_{\xi \xi} \\ & \quad + \frac{1}{\rho h_1 h_2} \frac{\partial h_2}{\partial \xi} \tau_{\eta \xi}, \end{aligned} \quad (5)$$

z -direction

$$\begin{aligned} & \frac{\partial w}{\partial t} + \frac{u}{h_1} \frac{\partial w}{\partial \xi} + \frac{v}{h_2} \frac{\partial w}{\partial \eta} + w \frac{\partial w}{\partial z} \\ &= -g \frac{\partial}{\partial z} \left(z + \frac{P}{\rho g} \right) + \frac{1}{\rho h_1 h_2} \left[\frac{\partial}{\partial \xi} (h_2 \tau_{z \xi}) + \frac{\partial}{\partial \eta} (h_1 \tau_{z \eta}) + \frac{\partial}{\partial z} (h_1 h_2 \tau_{zz}) \right], \end{aligned} \quad (6)$$

where ξ and η are the orthogonal curvilinear co-ordinates in the horizontal plane; z is the axis perpendicular to the ξ - η plane; h_1 is the metric coefficient in the ξ -direction; h_2 the metric coefficient in the η -direction; u the ξ component of velocity; v the η component of velocity; w the z component of velocity; g the gravitational acceleration; z the vertical position of a fluid particle; τ_{ij} a shear stress acting on the face that is perpendicular to the i -axis, and acting in the direction of the j -axis.

2.2. Depth-averaged equations

Natural watercourses may be described as the shallow water flows when the water depth is much less than the other two (horizontal) dimensions of the flow domain, i.e. the depth-to-width ratio is small. The vertical variation of velocity can be neglected, then the flow may be named as nearly horizontal flow. To obtain the two-dimensional depth-averaged equations, Equations (3)–(6) have to be integrated from the channel bottom to the water surface. And one needs to use the Leibnitz rule and the kinematic boundary conditions given by Equations (7) and (8) to evaluate these integrals.

The kinematic boundary condition at the channel bed is

$$\frac{\partial z_b}{\partial t} + \frac{u_b}{h_1} \frac{\partial z_b}{\partial \xi} + \frac{v_b}{h_2} \frac{\partial z_b}{\partial \eta} - w_b = 0; \quad (7)$$

The corresponding mean water surface boundary condition is

$$\frac{\partial z_s}{\partial t} + \frac{u_s}{h_1} \frac{\partial z_s}{\partial \xi} + \frac{v_s}{h_2} \frac{\partial z_s}{\partial \eta} - w_s = 0, \quad (8)$$

where subscripts s and b indicate the dependent variables at the water surface and channel bed respectively.

From order of magnitude analysis, the orders of magnitude of integrals of $\tau_{\xi \xi}$, $\tau_{\xi \eta}$, $\tau_{\eta \eta}$ and $\tau_{\eta \xi}$ are much less than that of bed friction. Neglecting these shear stresses in the momentum equations and considering static pressure distribution in the z -direction, one can obtain the depth-averaged two-dimensional equations in an orthogonal curvilinear co-ordinate system as follows:

$$h_1 h_2 \frac{\partial d}{\partial t} + \frac{\partial}{\partial \xi} (h_2 \bar{u} d) + \frac{\partial}{\partial \eta} (h_1 \bar{v} d) = 0, \quad (9)$$

$$\frac{\partial \bar{u}}{\partial t} + \frac{\bar{u}}{h_1} \frac{\partial \bar{u}}{\partial \xi} + \frac{\bar{v}}{h_2} \frac{\partial \bar{u}}{\partial \eta} + \frac{1}{h_1 h_2} \frac{\partial h_1}{\partial \eta} \bar{u} \bar{v} - \frac{1}{h_1 h_2} \frac{\partial h_2}{\partial \xi} \bar{v}^2 = -\frac{g}{h_1} \frac{\partial}{\partial \xi} (z_b + d) + \frac{\tau_{s\xi} - \tau_{b\xi}}{\rho d}, \tag{10}$$

$$\frac{\partial \bar{v}}{\partial t} + \frac{\bar{u}}{h_1} \frac{\partial \bar{v}}{\partial \xi} + \frac{\bar{v}}{h_2} \frac{\partial \bar{v}}{\partial \eta} + \frac{1}{h_1 h_2} \frac{\partial h_2}{\partial \xi} \bar{u} \bar{v} - \frac{1}{h_1 h_2} \frac{\partial h_1}{\partial \eta} \bar{u}^2 = -\frac{g}{h_2} \frac{\partial}{\partial \eta} (z_b + d) + \frac{\tau_{s\eta} - \tau_{b\eta}}{\rho d}, \tag{11}$$

$$\tau_{s\xi} = \tau_{s\eta} = 0, \tag{12}$$

$$\tau_{b\xi} = C_f \rho \bar{u} (\bar{u}^2 + \bar{v}^2)^{1/2}, \tag{13}$$

$$\tau_{b\eta} = C_f \rho \bar{v} (\bar{u}^2 + \bar{v}^2)^{1/2}, \tag{14}$$

where d , water depth; z_b , the elevation of the channel bottom; τ_{s_i} , τ_{b_i} , the i th-direction components of free-surface and bed shear stress; C_f , friction factor and the double overbar denotes depth averaging.

3. NUMERICAL ALGORITHM

3.1. Two-step split-operator approach

The present model uses a newly proposed two-step split-operator approach for solving shallow water flow equations. The advantages of this method are that the governing equations can be solved with primitive variables and the convergence rate can be accelerated by performing the computation only on a single pressure equation instead on a set of equations, including continuity and momentum equations. The procedure involves two steps based on a decomposition of the momentum equations. The first step, dispersion step, is to compute the provisional velocity in the momentum equation without the pressure gradient. Then the second step, propagation step, is to correct the provisional velocity by considering a divergence-free velocity field, including the effects of the pressure gradient and bed friction. They are expressed sequentially in the vector form as follows:

Dispersion step

$$\left(\frac{\partial \vec{v}}{\partial t} \right)^d = -(\vec{v} \cdot \nabla) \vec{v}^n. \tag{15}$$

Propagation step

$$\left(\frac{\partial \vec{v}}{\partial t} \right)^{n+1} - \left(\frac{\partial \vec{v}}{\partial t} \right)^d = -g \nabla (z_b + d)^{n+1} - \frac{\tau_{b_i}}{\rho d} \tag{16}$$

and

$$\nabla \cdot \vec{v}^{n+1} = 0. \tag{17}$$

One can express the above equations again in the orthogonal curvilinear co-ordinate system in the following steps and drop the double overbar to simplify the notation of depth-averaging for velocity variables.

Dispersion step

$$\frac{u^d - u^n}{\Delta t} = -\frac{u^n}{h_1} \cdot \left(\frac{\Delta u^n}{\Delta \xi} \right) - \frac{v^n}{h_2} \cdot \left(\frac{\Delta u^n}{\Delta \eta} \right) - \frac{1}{h_1 h_2} \left[\frac{\Delta h_1}{\Delta \eta} u^n v^n - \frac{\Delta h_2}{\Delta \xi} (v^n)^2 \right], \tag{18}$$

$$\frac{v^d - v^n}{\Delta t} = -\frac{u^n}{h_1} \cdot \left(\frac{\Delta v^n}{\Delta \xi} \right) - \frac{v^n}{h_2} \cdot \left(\frac{\Delta v^n}{\Delta \eta} \right) - \frac{1}{h_1 h_2} \left[\frac{\Delta h_2}{\Delta \xi} u^n v^n - \frac{\Delta h_1}{\Delta \eta} (u^n)^2 \right]. \tag{19}$$

Propagation step

$$\frac{u^{n+1} - u^d}{\Delta t} = -\frac{g}{h_1} \left[\frac{\partial}{\partial \xi} (z_b + d)^{n+1} \right] - \frac{C_f^n u^{n+1} \sqrt{(u^d)^2 + (v^d)^2}}{d^n}, \tag{20}$$

$$\frac{v^{n+1} - v^d}{\Delta t} = -\frac{g}{h_2} \left[\frac{\partial}{\partial \eta} (z_b + d)^{n+1} \right] - \frac{C_f^n v^{n+1} \sqrt{(u^d)^2 + (v^d)^2}}{d^n} \tag{21}$$

and

$$h_1 h_2 \frac{d^{n+1} - d^n}{\Delta t} + \frac{\partial}{\partial \xi} (h_2 u^{n+1} d^{n+1}) + \frac{\partial}{\partial \eta} (h_1 v^{n+1} d^{n+1}) = 0, \tag{22}$$

where u^d and v^d denote the provisional velocity for dispersion step; superscript n denotes the known variables at time level n and superscript $n + 1$ denotes the unknown variables at time level $n + 1$.

The expression of velocity at time level $n + 1$ can be rearranged from Equations (20) and (21) as follows:

$$u^{n+1} = \frac{1}{C_\tau} u^d - \frac{g \Delta t}{C_\tau h_1} \left[\frac{\partial}{\partial \xi} (z_b + d)^{n+1} \right], \tag{23}$$

$$v^{n+1} = \frac{1}{C_\tau} v^d - \frac{g \Delta t}{C_\tau h_2} \left[\frac{\partial}{\partial \eta} (z_b + d)^{n+1} \right], \tag{24}$$

$$C_\tau = 1 + \Delta t \frac{C_f^n \sqrt{(u^d)^2 + (v^d)^2}}{d^n}, \tag{25}$$

Using a Taylor series expansion for water depth, d^{n+1} , and retaining the first-order terms only, one can easily obtain the linearized expressions of (23) and (24) as follows:

$$(h_2 u d)^{n+1} = \alpha_1 \frac{\partial \Delta d}{\partial \xi} + \beta_1 \Delta d + \gamma_1, \tag{26}$$

$$(h_1 v d)^{n+1} = \alpha_2 \frac{\partial \Delta d}{\partial \eta} + \beta_2 \Delta d + \gamma_2, \tag{27}$$

where

$$\alpha_1 = -\frac{h_2 g \Delta t}{C_\tau h_1} d^n; \quad \beta_1 = \frac{h_2}{C_\tau} u^d - \frac{h_2 g \Delta t}{C_\tau h_1} \left[\frac{\partial z_b^{n+1}}{\partial \xi} + \frac{\partial d^n}{\partial \xi} \right]; \quad \gamma_1 = \beta_1 d^n, \tag{28}$$

$$\alpha_2 = -\frac{h_1 g \Delta t}{C_\tau h_2} d^n; \quad \beta_2 = \frac{h_1}{C_\tau} v^d - \frac{h_1 g \Delta t}{C_\tau h_2} \left[\frac{\partial z_b^{n+1}}{\partial \eta} + \frac{\partial d^n}{\partial \eta} \right]; \quad \gamma_2 = \beta_2 d^n. \tag{29}$$

Substituting Equations (26) and (27) into (22) leads to

$$h_1 h_2 \frac{\Delta d}{\Delta t} + \frac{\partial}{\partial \xi} \left(\alpha_1 \frac{\partial \Delta d}{\partial \xi} + \beta_1 \Delta d + \gamma_1 \right) + \frac{\partial}{\partial \eta} \left(\alpha_2 \frac{\partial \Delta d}{\partial \eta} + \beta_2 \Delta d + \gamma_2 \right) = 0, \tag{30}$$

where $\Delta d = d^{n+1} - d^n$.

Equation (30) is called herein the depth increment equation. One should note that the idea behind the derivation of the depth increment equation is basically the same as that for the derivation of the ‘pressure equation’ used in projection method.

3.2. Discretized equations

Figure 1 shows the flow domain in the computational space. The solid lines represent the main grid and the broken lines represent the staggered grid. The water depth will be computed at main grid points that are denoted by small triangles in Figure 1. The zone with inclined lines whose faces lie on the staggered grid around a main grid point denotes the control volume. Along the boundary of control volume, the velocity components u and v will be computed at the staggered grid points. Then one can integrate the governing equations over the control volume to obtain the discretized equations. The same result could be obtained by using a finite difference scheme based on a Taylor series formulation. Such a staggered grid system was first used by Harlow and Welch [15] in their marker and cell (MAC) method. One of the important advantages is the avoidance of appearing wavy velocity fields. The discretized forms of the governing equations are given in the following paragraphs.

Dispersion step

The discretized equations from Equations (18) and (19) can be written as follows:

ξ -direction

$$\begin{aligned} \frac{u_{i+1/2,j}^d - u_{i+1/2,j}^n}{\Delta t} = & -\frac{u_{i+1/2,j}^n}{h_{1i+1/2,j}} \cdot 0.5 \cdot \left[(1 - \alpha_x) \left(\frac{u_{i+3/2,j}^n - u_{i+1/2,j}^n}{\Delta \xi} \right) \right. \\ & \left. + (1 + \alpha_x) \left(\frac{u_{i+1/2,j}^n - u_{i-1/2,j}^n}{\Delta \xi} \right) \right] \\ & - \frac{v_{i+1/2,j}^n}{h_{2i+1/2,j}} \cdot 0.5 \cdot \left[(1 - \alpha_y) \left(\frac{u_{i+1/2,j+1}^n - u_{i+1/2,j}^n}{\Delta \eta} \right) \right. \\ & \left. + (1 + \alpha_y) \left(\frac{u_{i+1/2,j}^n - u_{i+1/2,j-1}^n}{\Delta \eta} \right) \right] \\ & - \frac{1}{h_{1i+1/2,j} h_{2i+1/2,j}} \left[\frac{h_{1i+1/2,j+1/2} - h_{1i+1/2,j-1/2}}{\Delta \eta} (u_{i+1/2,j}^n v_{i+1/2,j}^n) \right. \\ & \left. - \frac{h_{2i+1,j} - h_{2i,j}}{\Delta \xi} (v_{i+1/2,j}^n)^2 \right], \end{aligned} \tag{31}$$

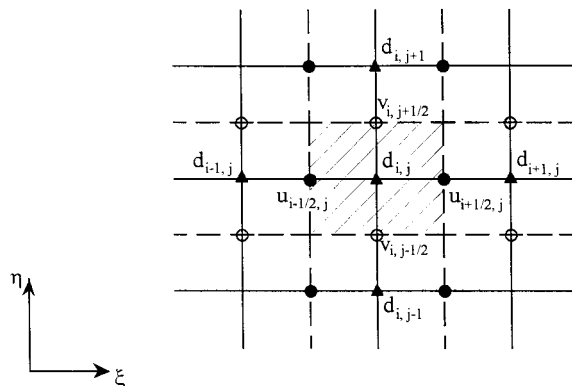


Figure 1. Computational domain with staggered grid.

η -direction

$$\begin{aligned} \frac{v_{i,j+1/2}^d - v_{i,j+1/2}^n}{\Delta t} = & -\frac{u_{i,j+1/2}^n}{h_{1i,j+1/2}} \cdot 0.5 \cdot \left[(1 - \alpha_x) \left(\frac{v_{i+1,j+1/2}^n - v_{i,j+1/2}^n}{\Delta \xi} \right) \right. \\ & \left. + (1 + \alpha_x) \left(\frac{v_{i,j+1/2}^n - v_{i-1,j+1/2}^n}{\Delta \xi} \right) \right] \\ & - \frac{v_{i,j+1/2}^n}{h_{2i,j+1/2}} \cdot 0.5 \cdot \left[(1 - \alpha_y) \left(\frac{v_{i,j+3/2}^n - v_{i,j+1/2}^n}{\Delta \eta} \right) \right. \\ & \left. + (1 + \alpha_y) \left(\frac{v_{i,j+1/2}^n - v_{i,j-1/2}^n}{\Delta \eta} \right) \right] \\ & - \frac{1}{h_{1i,j+1/2} h_{2i,j+1/2}} \left[\frac{h_{2i+1/2,j+1/2} - h_{2i-1/2,j+1/2}}{\Delta \xi} (u_{i,j+1/2}^n v_{i,j+1/2}^n) \right. \\ & \left. - \frac{h_{1i+1,j} - h_{1i,j}}{\Delta \eta} (u_{i,j+1/2}^n)^2 \right], \end{aligned} \tag{32}$$

where

$$\alpha_x = \begin{cases} 0 & |R_x| \leq 2 \\ 1 & R_x > 2 \\ -1 & R_x < -2 \end{cases}; \quad \alpha_y = \begin{cases} 0 & |R_y| \leq 2 \\ 1 & R_y > 2 \\ -1 & R_y < -2 \end{cases}, \tag{33}$$

$$R_x = \frac{u_{i+1/2,j}^n h_{1i+1/2,j} \Delta \xi}{\mu / \rho}; \quad R_y = \frac{v_{i+1/2,j}^n h_{2i+1/2,j} \Delta \eta}{\mu / \rho}, \tag{34}$$

μ is the fluid dynamic viscosity.

The hybrid scheme [16] that combines the central difference and the upwind scheme is used herein for calculating the advection terms to catch the direction of fluid flow. The mesh Reynolds number (R_x or R_y) introduced in the algorithm is to help select the proper finite difference mode for computing the advection terms. The central difference is used in the low mesh Reynolds number and the upwind scheme is used in the high mesh Reynolds number. The upwind scheme uses backward difference when the velocity is positive and uses forward difference when the velocity is negative. The hybrid scheme provides the first-order accuracy against the upwind scheme and second-order accuracy against central difference in the space. Meanwhile, the numerical parameters α_x and α_y are used to automatically shift to the proper mode, depending on the strength of advection effects through the judgment of the magnitude of mesh Reynolds number and the direction of fluid flow.

If the implicit scheme is used for Equations (31) and (32), the accuracy of the solution in the propagation step will be dependent on the provisional velocity u_Γ^d at the boundary in the dispersion step [13]. Therefore, the explicit scheme is used here to discretize Equations (31) and (32). One can choose $u_\Gamma^d = u_\Gamma^n$ (i.e. previous step velocity) to avoid the problem caused by the unknown velocity at the boundary Γ in the dispersion step. The advantage of this treatment is that the solution is independent of the velocity at boundary, u_Γ^d .

Propagation step

The discretized forms of the differential equations (23), (24) and (30) can be expressed respectively, as follows

$$\begin{aligned} & h_{1i,j} h_{2i,j} \frac{\Delta d_{i,j}}{\Delta t} + \{ [\alpha_{1i+1/2,j} (\Delta d_{i+1,j} - \Delta d_{i,j}) + \beta_{1i+1/2,j} \Delta d_{i+1/2,j} + \gamma_{1i+1/2,j}] \\ & - [\alpha_{1i-1/2,j} (\Delta d_{i,j} - \Delta d_{i-1,j}) + \beta_{1i-1/2,j} \Delta d_{i-1/2,j} + \gamma_{1i-1/2,j}] \} / \Delta \xi \end{aligned}$$

$$+ \{[\alpha_{2_{i,j+1/2}}(\Delta d_{i,j+1} - \Delta d_{i,j}) + \beta_{2_{i,j+1/2}}\Delta d_{i,j+1/2} + \gamma_{2_{i,j+1/2}}] - [\alpha_{2_{i,j-1/2}}(\Delta d_{i,j} - \Delta d_{i,j-1}) + \beta_{2_{i,j-1/2}}\Delta d_{i,j-1/2} + \gamma_{2_{i,j-1/2}}]\} / \Delta \eta = 0, \tag{35}$$

$$u_{i+1/2,j}^{n+1} = \frac{1}{C_{\tau_{i+1/2,j}}} u_{i+1/2,j}^d - \frac{g\Delta t}{C_{\tau_{i+1/2,j}} h_{1i+1/2,j}} [(z_b + d)_{i+1,j}^{n+1} - (z_b + d)_{i,j}^{n+1}], \tag{36}$$

$$v_{i,j+1/2}^{n+1} = \frac{1}{C_{\tau_{i,j+1/2}}} v_{i,j+1/2}^d - \frac{g\Delta t}{C_{\tau_{i,j+1/2}} h_{2i,j+1/2}} [(z_b + d)_{i,j+1}^{n+1} - (z_b + d)_{i,j}^{n+1}]. \tag{37}$$

The ADI method is used to solve Equation (35) iteratively until the solution is converged. The final velocities from Equations (36) and (37) at time level $n + 1$ can be computed explicitly after Equation (35), which has been solved.

3.3. Boundary conditions

Equation (35) requires boundary conditions to enclose the partial differential equation problem. In general, an unit discharge hydrograph at the upstream end and a water surface variation at the downstream end are very common boundary conditions for the subcritical flows. And the impermeable condition is used for the bank of channel. These types of boundary conditions are easy to transform into the function of depth increment variable. It is more convenient to directly obtain the depth increment at the boundary from Equation (35). For instance, a unit discharge in the ξ -direction can be expressed as the function of depth increment, like in Equation (26), then the coefficient matrix of Equation (35) at the upstream boundary can be determined by comparing it with the coefficient of Equation (26). The derivation of coefficient for the upstream boundary is briefly introduced in Appendix A.

3.4. Overall solution procedure

The solution procedures for solving shallow water flow equations can be listed as follows:

1. Calculate the provisional velocities (u^d, v^d) explicitly from the momentum equations (31) and (32) without the pressure gradient terms to complete dispersion step.
2. Compute Equation (35) implicitly to obtain depth increment (Δd) by the ADI method.
3. The unknown velocities (u^{n+1}, v^{n+1}) are calculated by correcting the provisional velocities with the pressure gradient and bed friction from Equations (36) and (37) to complete the propagation step.
4. Return to step 1 and proceed to the next time step.
5. Repeat procedures 1–4 until a steady state solution is reached (for steady state flows) or the specific time period is completed (for unsteady flows).

4. DEMONSTRATION

In order to verify the capability of the two-step split-operator approach used for solving shallow water flow equations, four cases, including back-water flow, reverse flow, circular basin flow and unsteady flow, are studied herein. Because of using an explicit scheme in the dispersion step, the stability of solution is determined from the Courant–Friedrichs–Lewy (CFL) condition:

$$CFL = \max_{i,j} \left[\left(\frac{|u_{i,j}|}{\Delta x_i} + \frac{|v_{i,j}|}{\Delta y_i} \right) \Delta t \right] < 1. \tag{38}$$

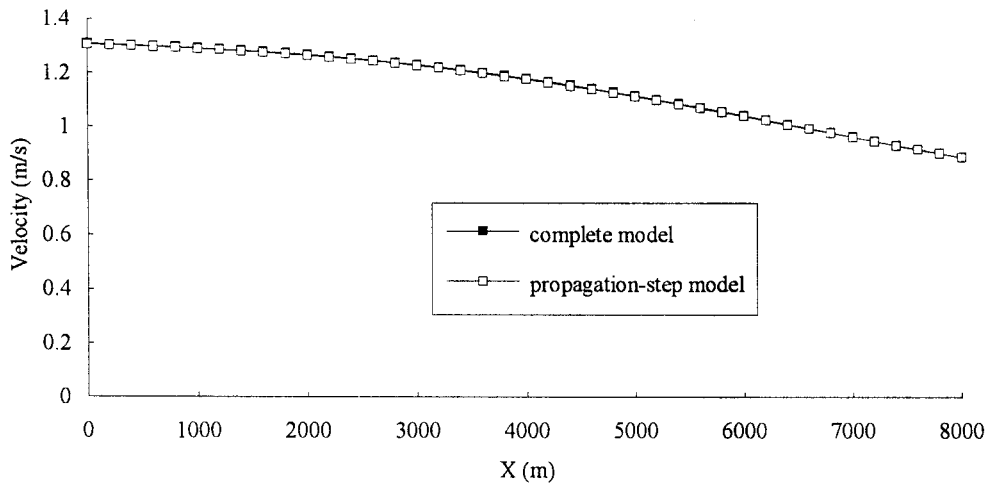


Figure 2. The variation of velocity along the channel for back-water flow case.

In all cases, the grid systems are constructed to be fine enough to meet the requirement of reasonable accuracy as well as execution time.

4.1. Back-water flow case

A steady non-uniform flow in a prismatic channel with gradual changes in its water surface elevation is written as the gradually varied flow (GVF). The back-water flow caused by a dam or weir across a river as a control section at the downstream of river is one of the typical examples of GVF. In the GVF case, the velocity varies along the channel; consequently, the bed slope, water surface slope and energy slope will be different from one another in each section. Standard step method based on trial and error solution of basic energy equation is a common numerical solution procedure to calculate the GVF profile, that is also included in many well-known commonly used models, such as the HEC-2 [17] model. The computation of back-water flow is one of the standard tests for examining the proposed method for the shallow water flow equations.

A rectangular channel with a length of 8000 m, a width of 100 m, a slope of 0.005, and a Manning's roughness of 0.035 has been considered here for study. The depth of flow is 3.0 m and the unit discharge of steady inflow is $3.987 \text{ m}^3 \text{ s}^{-1} \text{ m}^{-1}$. At the outlet of the channel, the water surface will be raised to 4.5 m by a low weir as a control. The critical depth of this flow is 1.175 m, so the back-water profile is an M_1 curve.

The space intervals $\Delta x = 200.0 \text{ m}$, $\Delta y = 20.0 \text{ m}$ and time interval $\Delta t = 200 \text{ s}$ are used. The simulated variations of velocity and flow depth are shown in Figures 2 and 3 respectively. From Figure 3, one can observe that the flow depth gradually varies from 4.5 m at weir to 3.05 m at the upstream closed to the normal depth. Consequently, as shown in Figure 2, the velocity varies from 0.886 m s^{-1} to 1.307 m s^{-1} , corresponding with the variation of flow depth from downstream to upstream. The simulated results from the complete model (including the dispersion and propagation steps) are compared with results from the propagation step model (only propagation step used) to demonstrate their characteristics. From Figures 2 and 3, it is obvious that the complete model and propagation step model have the same results. One can easily discern that the simulated performance from the propagation step model is the

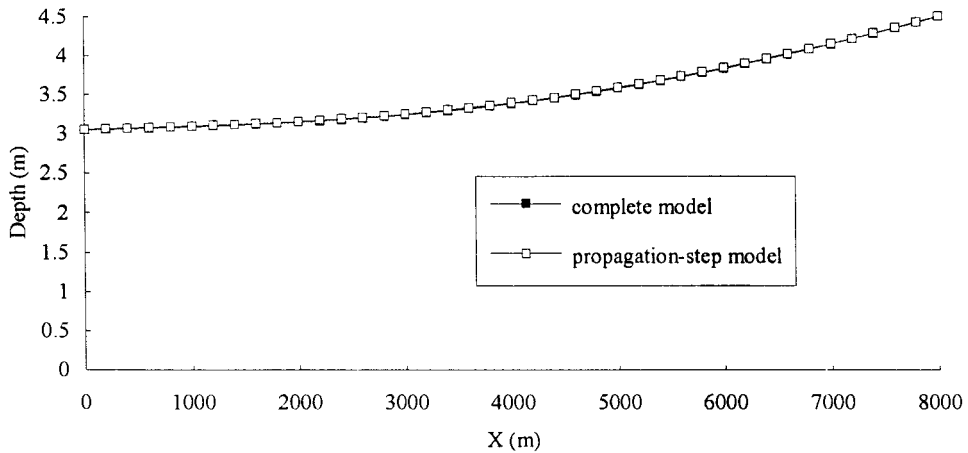


Figure 3. The variation of water depth along the channel for back-water flow case.

same from the standard step method by solving the energy equation. In brief, when the effect of advection is weak, propagation step model can handle GVF case well and reduce about 70% of CPU time as compared with the complete model.

4.2. Reverse flow case

In order to identify the importance of advective terms in the momentum equations, a compound channel with gradual expanding width is considered, as shown in Figure 4. The channel with a slope of 0.005 is 2000 m long and its width gradually expands from 100 m at the inlet to 260 m at the outlet. The Manning’s roughness of the channel is 0.035. Along the longitudinal channel, there exists a main deep channel in which the cross-section of the compound channel is symmetric. The width of the main deep channel expands from 40 to 104

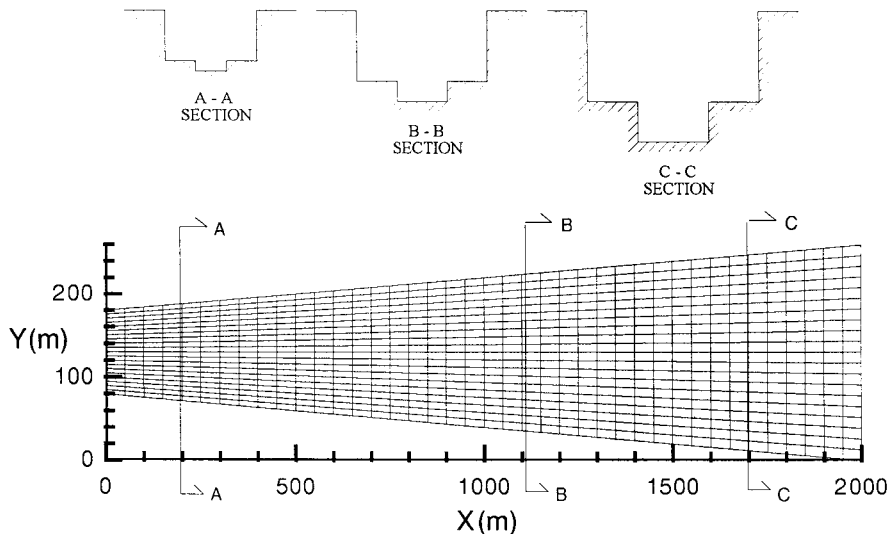


Figure 4. The plain view of compound channel.

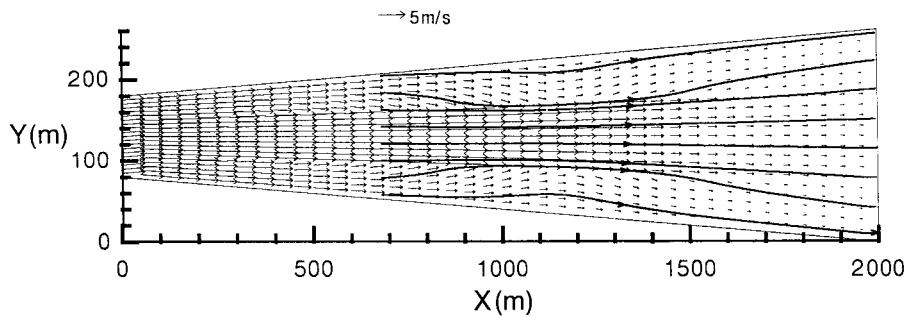


Figure 5. Sketch of velocity vector and streamline by the propagation step model ($q = 10 \text{ m}^3 \text{ s}^{-1} \text{ m}^{-1}$).

m; and the slope of channel is 0.007. A steady unit discharge of $10 \text{ m}^3 \text{ s}^{-1} \text{ m}^{-1}$ is given at the inlet of channel. The flow depth of 8 m from the bottom of main deep channel is given at the outlet.

A mesh of 41×21 is used for the computational domain. The velocity fields computed by the propagation step and complete models are shown in Figures 5 and 6 respectively. One may note that Figures 5 and 6 demonstrate the different flow patterns near the downstream of the channel, a reverse flow can clearly be observed in Figure 6, but not in Figure 5. The velocity speeds up along the main deep channel owing that the main deep channel is steeper than the flood plain. In Figure 5, the velocity near the downstream in the main deep channel diverges outwards to the lateral bank of channel and slows down. However, Figure 6 shows the velocity remains in the main deep channel by the complete model, and the water level in the main deep channel decreases corresponding with higher velocity near the downstream. This may cause the phenomena of reverse flow near the outlet of the channel. The propagation step model cannot simulate the reverse flow pattern. This is simply because the flow direction of advection can not be caught by the propagation step computing without considering advection terms. On the other hand, when the inflow unit discharge is raised up to $30 \text{ m}^3 \text{ s}^{-1} \text{ m}^{-1}$ and the other simulated conditions are retained, due to the strong advection effect, the reverse flow phenomenon near the downstream vanish even with the use of the complete model, as shown in Figure 7. In order to further examine the difference between the complete model and the propagation step model and to show the capability of two-step split-operator approach, a circular basin flow case is studied in the following paragraphs.

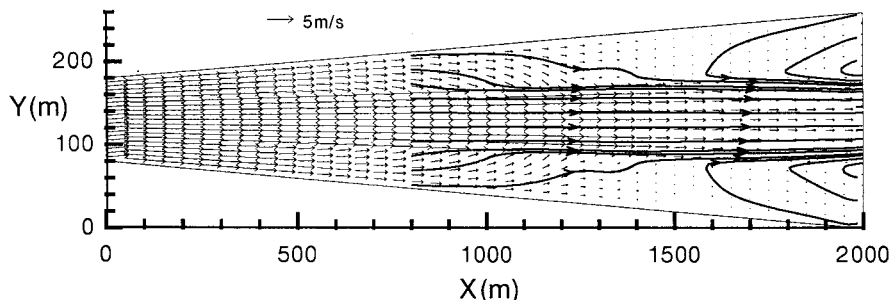


Figure 6. Sketch of velocity vector and streamline by the complete model ($q = 10 \text{ m}^3 \text{ s}^{-1} \text{ m}^{-1}$).

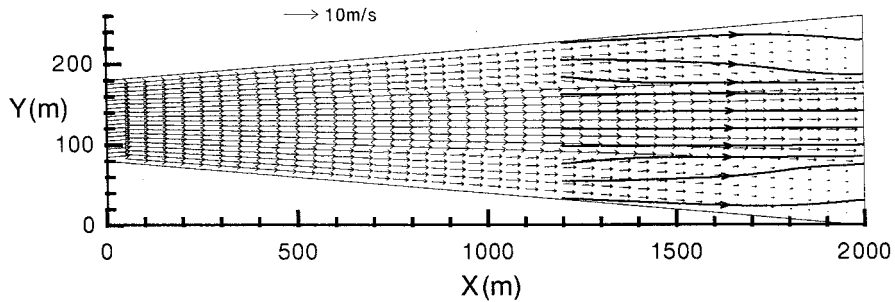


Figure 7. Sketch of velocity vector and streamline by the complete model ($q = 30 \text{ m}^3 \text{ s}^{-1} \text{ m}^{-1}$).

4.3. Circular basin flow case

While the jet-forced flow is induced into a reservoir, a mixing of circular flow will prevent the stagnation in shallow service reservoirs. Such flow in a circular reservoir is separated and contains recirculating gyres. Therefore, the simulation of jet-forced flow in a circular reservoir is a useful test to validate the effect of advective acceleration terms in the momentum equations. Falconer [18] solved the shallow water flow equations in terms of a Cartesian co-ordinate system using a semi-implicit finite difference scheme and a stepped approximation to the curved boundaries for a circular basin. Barber [19], and Borthwick and Akponasa [20] used non-orthogonal boundary fitted systems versions of the shallow water flow equations to eliminate boundary alignment errors.

Falconer [1] conducted an experiment in which the geometry of the basin is circular, with vertical side walls and a flat bottom. As shown in Figure 8, the inlet width is 0.08 m, the outlet width is 0.24 m, and the diameter is 1.5 m. The average depth of flow is 0.093 m and Chezy's coefficient of 43.8 is used. The discharge, $0.009375 \text{ m}^3 \text{ s}^{-1} \text{ m}^{-1}$ (750 cc s^{-1}), was continually supplied at the inlet until a steady predetermined discharge was recorded at the weir outlet. The circulatory flow patterns within the reservoir were governed by a jet inlet and a diametrically opposite weir outlet.

The orthogonal grid of the physical model is shown in Figure 8. These grids (51×23) are generated by algebraic grid generation method [21]. The simulated velocity vector by the

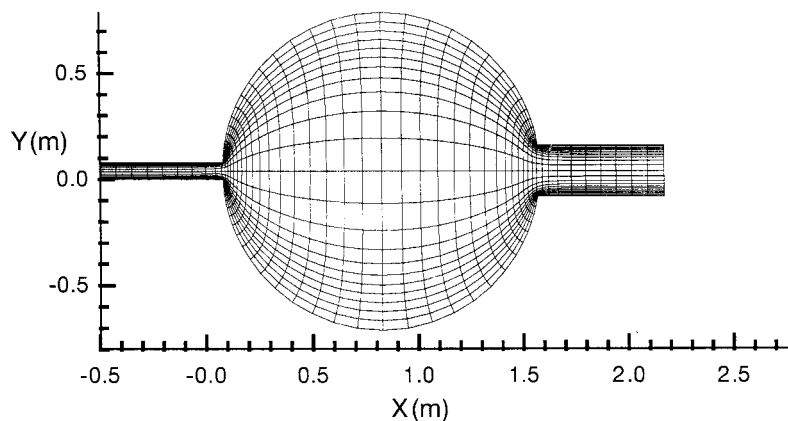


Figure 8. Physical grid system for circular basin flow case.

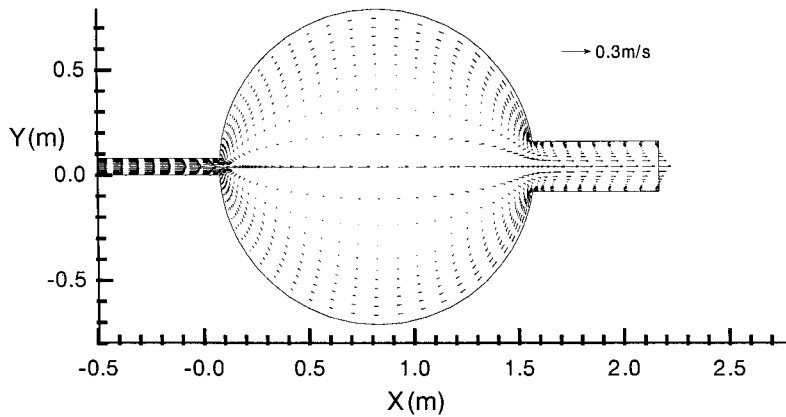


Figure 9. Velocity vector by the complete model for circular basin flow case.

complete model and the propagation step model are shown in Figures 9 and 10 respectively. The difference obviously exists in these results. Figure 9 shows the circulatory flow patterns within the circular basin as it can be observed in the physical model, but Figure 10 shows no recirculating gyres. It is evident that for such jet-forced flow, the circulation patterns, which are known to exist in the laboratory experiment, cannot be reproduced without calculating the advection terms. Figures 11 and 12 show the depth contours by the complete model and the propagation step model respectively. The water depth computed by the complete model near the inlet is 0.093 m, which is very close to the experimental data. In contrast, the result computed by the propagation step model is 0.091 m, which is below the averaged flow depth, therefore, reverse flow takes place in the circular basin. Maybe one of possible reasons is that the momentum can not be transferred to the center region of the circular basin without calculating the dispersion step. The complete model has agreeable results with measured data as shown in Figure 9. Benque *et al.* [4] simulated the same case, but the velocity was accelerated near the entrance of the circular basin, which is not shown in the experimental data. In short, the computed results show that it is inadequate for simulating circulation in circular basin without taking advection effects into account, especially when jet-forced effects

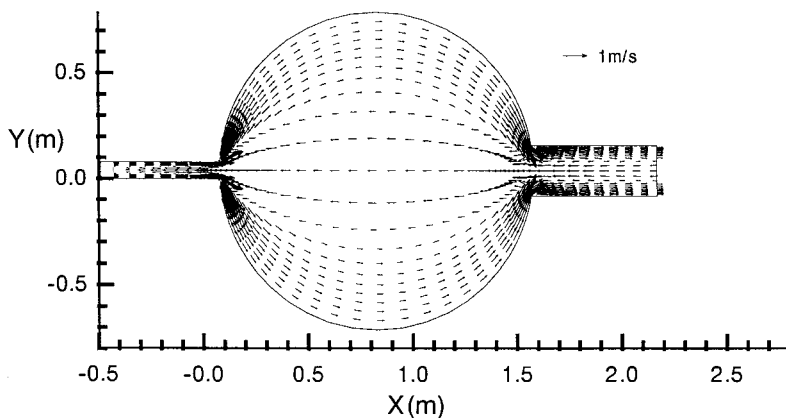


Figure 10. Velocity vector by the propagation step model for circular basin flow case.

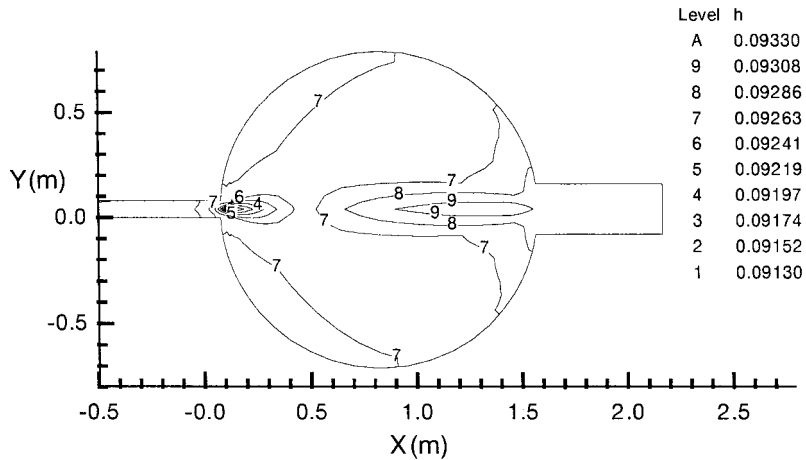


Figure 11. Depth contour by the complete model for circular basin flow case.

are strong. Through the comparison with the experimental data, one may be able to conclude that the two-step split-operator approach, which gives acceptably accurate results, should be a competitive scheme for developing 2D shallow water flow model.

4.4. Unsteady flow case

A simple hypothetical unsteady flow case has been considered herein to demonstrate the capability of the two-step split-operator approach for solving the time-dependent shallow water flow equations.

A straight channel with a length of 100 km, a width of 100 m, a slope of 0.0001 and the Manning's roughness of 0.0187 are assumed herein. An unit discharge hydrograph of flood flow, which is given at the inlet of channel as an upstream boundary condition, can be expressed as follows:

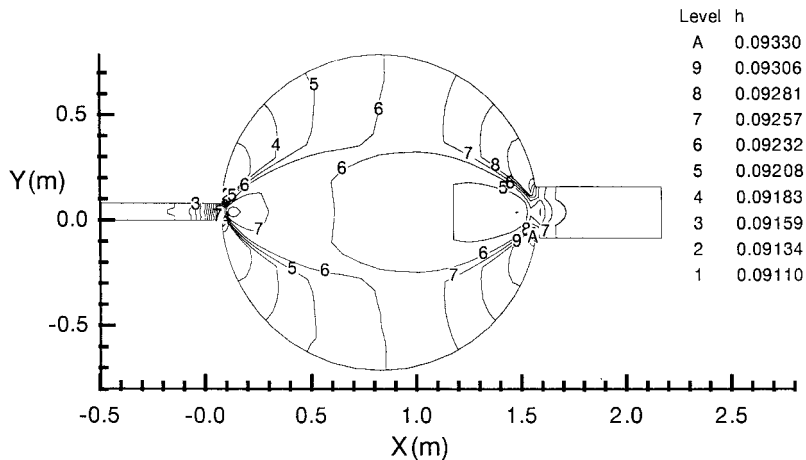


Figure 12. Depth contour by the propagation step model for circular basin flow case.

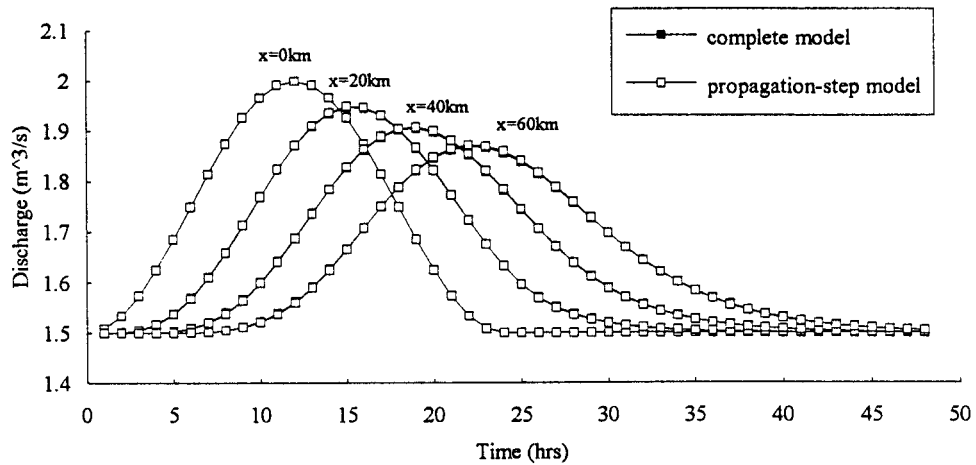


Figure 13. Discharge hydrograph at various predetermined locations for unsteady flow case.

$$q = \begin{cases} q_b + 0.5(q_p - q_b) \left[1 - \cos\left(\frac{2\pi t}{T}\right) \right] & 0 < t < 24 \text{ h} \\ q_b & 24 \text{ h} < t < 48 \text{ h} \end{cases}, \quad (39)$$

where q_b is the unit base discharge ($= 1.5 \text{ m}^3 \text{ s}^{-1} \text{ m}^{-1}$); q_p is the unit peak discharge ($= 2.0 \text{ m}^3 \text{ s}^{-1} \text{ m}^{-1}$); t is the time and T the duration, here taken as 24 h.

The grid size $\Delta x = 1000.0 \text{ m}$ and $\Delta y = 12.5 \text{ m}$ and time interval $\Delta t = 240 \text{ s}$ are used herein. The simulated time period is 48 h. Figures 13 and 14 show the simulated unit discharge and flow depth varied with time at 0, 20, 40 and 60 km from the upstream end respectively. One can observe that considerable attenuation has taken place, as well as a substantial time lag between the inflow and outflow peaks. Results obtained from both the complete model and the

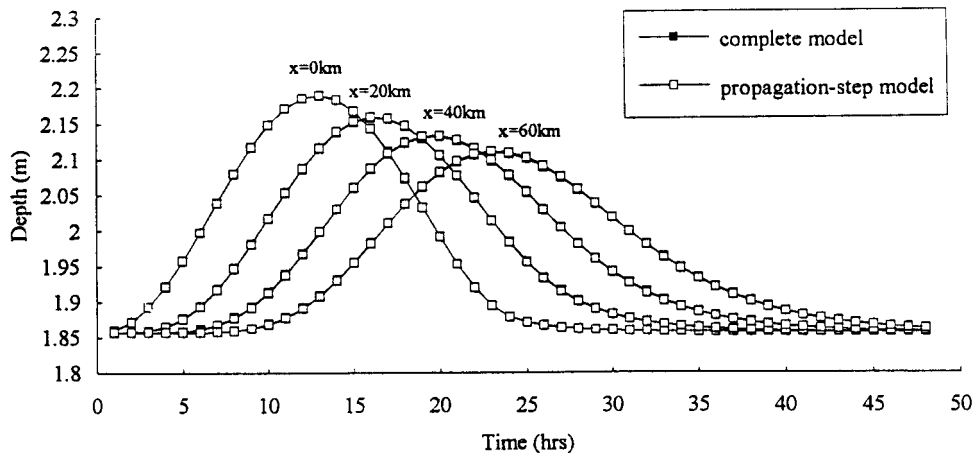


Figure 14. Water depth hydrograph at various predetermined locations for unsteady flow case.

propagation step model are compared in Figures 13 and 14. From these two figures, one can see that the complete model and the propagation step model give the same results when the advection effect is weak in the designed case. It may be because the flood movement is dominated by storage effects, the importance of the advective acceleration terms in the equations of motion can be reduced. The simulated results from this case have demonstrated the capability of the split-operator approach for the unsteady flow simulation.

5. CONCLUSIONS

A new two-step split-operator solution procedure for solving the shallow water flow equations has been presented in this paper. The procedure involves two steps based on a decomposition of the momentum equations. The first step (dispersion step) is to compute the provisional velocity in the momentum equation without the pressure gradient. The second step (propagation step) is to correct the provisional velocity by considering a divergence-free velocity field including the effects of the pressure gradient and bed friction. Four cases, including back-water flow, reverse flow, circular basin flow and unsteady flow, have been demonstrated to show the flexibility and practical use of the method. In the back-water flow case, when the effect of advection is weak, the propagation step model can handle the GVF case well and reduce CPU time by about 70% as compared with the complete model. The cases of reverse flow and circular basin flow are good examples to identify the importance of advective terms in the momentum equations. These cases show that it is inadequate in attempting to simulate circulation in reservoirs without taking the momentum advection into account, especially when the jet-forced effects exist. The unsteady flow case demonstrates that the two-step split-operator approach is capable of solving the time-dependent shallow water flow equations with adequate accuracy. In summary, from the studies demonstrated previously, one may conclude that the new two-step split-operator approach proposed in this paper is a competitive scheme with the capability of being very flexible and applicable to all kinds of practical hydraulic problems.

ACKNOWLEDGMENTS

The financial support of this study from the National Science Council of Taiwan, Republic of China, through the Contract NSC-84-2211-E009-033 is greatly appreciated.

APPENDIX A

Equation (35) can be rearranged into the form:

$$a_p \Delta d_{i,j} + a_w \Delta d_{i-1,j} + a_E \Delta d_{i+1,j} + a_S \Delta d_{i,j-1} + a_N \Delta d_{i,j+1} = b_{i,j}, \quad (40)$$

where

$$a_w = \alpha_{1_{i-1/2,j}} - \frac{1}{2} \beta_{1_{i-1/2,j}}, \quad (41)$$

$$a_E = \alpha_{1_{i+1/2,j}} + \frac{1}{2} \beta_{1_{i+1/2,j}}, \quad (42)$$

$$a_S = \alpha_{2_{i,j-1/2}} - \frac{1}{2} \beta_{2_{i,j-1/2}}, \quad (43)$$

$$a_N = \alpha_{2_{i,j+1/2}} + \frac{1}{2} \beta_{2_{i,j+1/2}}, \quad (44)$$

$$a_P = \frac{h_{1_{i,j}} h_{2_{i,j}}}{\Delta t} - a_W - a_E - a_S - a_N, \quad (45)$$

$$b_{i,j} = \gamma_{1_{i-1/2,j}} - \gamma_{1_{i+1/2,j}} + \gamma_{2_{i,j-1/2}} - \gamma_{2_{i,j+1/2}}. \quad (46)$$

As a unit discharge was imposed at the upstream boundary, Equation (26) can be rearranged at the inlet ($i=1$) as follows,

$$\begin{aligned} & \left(\alpha_{1_{i+1/2,j}} + \frac{1}{2} \beta_{1_{i+1/2,j}} \right) \Delta d_{i,j} + \left(-\alpha_{1_{i+1/2,j}} + \frac{1}{2} \beta_{1_{i+1/2,j}} \right) \Delta d_{i+1,j} \\ & = -\gamma_{1_{i+1/2,j}} + h_{2_{i+1/2,j}} Q(t^{n+1}), \end{aligned} \quad (47)$$

so the coefficient matrix at the upstream boundary for the unit discharge are,

$$a_P = \alpha_{1_{i+1/2,j}} + \frac{1}{2} \beta_{1_{i+1/2,j}}; \quad a_E = -\alpha_{1_{i+1/2,j}} + \frac{1}{2} \beta_{1_{i+1/2,j}};$$

$$b_{i,j} = -\gamma_{1_{i+1/2,j}} + h_{2_{i+1/2,j}} Q(t^{n+1})$$

and the others are zero.

REFERENCES

1. R.A. Falconer, 'Numerical modeling of tidal circulation in harbors', *J. Waterw. Port Coast. Ocean Div. ASCE*, **106**, 31–48 (1980).
2. T. Takahashi and H. Nakagawa, 'Hazard zone mapping in respect to the damages to wooden house due to breaking of levee', *Bulletin 37*, Disaster Prevention Research Institute, Kyoto University, Japan, 1987, pp. 59–90.
3. T. Molls and M.H. Chaudhry, 'Depth-averaged open-channel flow model', *J. Hydraul. Eng. ASCE*, **121**, 453–465 (1995).
4. J.P. Benque, J.A. Cunge, J. Feuillet, A. Hauguel and F.M. Holly, 'New method for tidal current computation', *J. Waterw. Port Coast. Ocean Div. ASCE*, **108**, 396–417 (1982).
5. J. Ye and J.A. McCorquodale, 'Depth-averaged hydrodynamic model in curvilinear collocated grid', *J. Hydraul. Eng. ASCE*, **123**, 380–388 (1997).
6. M. Fortin, R. Peyret and R. Temam, *Lecture Notes in Physics*, vol. 8, Springer, New York, 1971, pp. 337–342.
7. T.L. Lee and T.F. Lin, 'Transient three-dimensional convection of air in a differentially heated rotating cubic cavity', *Int. J. Mass Transf.*, **39**, 1243–1255 (1996).
8. M. Rosenfeld, D. Kwak and M. Vinokur, 'A fractional step solution method for the unsteady incompressible Navier–Stokes equations in generalized co-ordinate systems', *J. Comput. Phys.*, **94**, 102–137 (1991).
9. S.V. Pantankar, *Numerical Heat Transfer and Fluid Flow*, Hemisphere Publishing, Bristol, PA, 1980.
10. M. Rosenfeld and D. Kwak, 'Multigrid acceleration of a fractional step solver in generalized curvilinear co-ordinate systems', *AIAA J.*, **31**, 1792–1800 (1993).
11. M. Spasojevic and F.M. Holly, '2D bed evolution in natural watercourses—new simulation approach', *J. Waterw. Port Coast. Ocean. Eng. ASCE*, **116**, 425–433 (1990).
12. J.P. Van Doormaal and G.D. Raithby, 'Enhancements of the SIMPLER method for predicting incompressible fluid flows', *Numer. Heat Transf.*, **7**, 147–163 (1984).
13. R. Preyter and T.D. Taylor, *Computational Methods for Fluid Flow*, Springer, New York, 1983, pp. 160–162.
14. D.A. Anderson, J.C. Tannehill and R.H. Pletcher, *Computational Fluid Mechanics and Heat Transfer*, Hemisphere Publishing, Bristol, PA, 1984.
15. F.H. Harlow and J.E. Welch, 'Numerical calculation of time-dependent viscous incompressible flow of fluid with free surface', *Phys. Fluids*, **8**, 2182–2189 (1965).
16. D.B. Spalding, 'A novel finite difference formulation for differential expressions involving both first and second derivatives', *Int. J. Numer. Methods Eng.*, **4**, 551–559 (1972).
17. Hydrologic Engineering Center, *Water Surface Profile*, Computer Program HEC-2, US Army Corps of Engineers, Davis, CA, 1982.
18. R.A. Falconer, 'Mathematical modeling of jet-forced circulation in reservoirs and harbours', *Ph.D. Thesis*, Imperial College, London, 1976.

19. R.W. Barber, 'Numerical modeling of jet-forced circulation in reservoirs using boundary fitted co-ordinate systems', *Ph.D. Thesis*, Salford University, UK, 1990.
20. A.G.L. Borthwick and G.A. Akponasa, 'Reservoir flow prediction by contravariant shallow water equations', *J. Hydraul. Eng. ASCE*, **123**, 432–439 (1997).
21. Y.N. Jeng and Y.L. Liou, 'A comparison between the algebraic grid generation method and methods using parabolic and hyperbolic partial differential equations', in B.K. Soni, J.F. Thompson and P. Eiseman (eds.), *Proc. 5th Int. conf. on Numerical Grid Generation in Computational Field Simulation*, Mississippi State University, 1996, pp. 157–166.